NOx degradation by photocatalytic mortars: the underlying role of the CH and C-S-H carbonation

Citation for published version (APA):
Kaja, A., Brouwers, J., & Yu, Q. (2019). NOx degradation by photocatalytic mortars: the underlying role of the CH and C-S-H carbonation. *Cement and Concrete Research*, *125*, Article 105805.
https://doi.org/10.1016/j.cemconres.2019.105805

Document license:
TAVERNE

DOI:
10.1016/j.cemconres.2019.105805

Document status and date:
Published: 01/11/2019

Document Version:
Publisher's PDF, also known as Version of Record (includes final page, issue and volume numbers)

Please check the document version of this publication:

• A submitted manuscript is the version of the article upon submission and before peer-review. There can be important differences between the submitted version and the official published version of record. People interested in the research are advised to contact the author for the final version of the publication, or visit the DOI to the publisher's website.
• The final author version and the galley proof are versions of the publication after peer review.
• The final published version features the final layout of the paper including the volume, issue and page numbers.

[Link to publication](#)

NOₓ degradation by photocatalytic mortars: The underlying role of the CH and C-S-H carbonation

A.M. Kaja, H.J.H. Brouwers, Q.L. Yu*

Department of the Built Environment, Eindhoven University of Technology, Eindhoven 5600, MB, the Netherlands

ABSTRACT

This study aims to understand the impact of carbonation mechanism of C-S-H and CH in photocatalytic mortars on NOₓ removal efficiency. Changes in surface chemistry and microstructure induced by the carbonation of portlandite and C-S-H (AFm/AFt) were correlated with the photocatalytic efficiency of the mortars doped with three types of titania-based photocatalysts. Furthermore, the influence of cementitious matrix on the photocatalytic selectivity was evaluated by studying the capacity of hydration/carbonation products to adsorb NO_2. The study revealed that in terms of both photocatalytic efficiency and selectivity, mortars with microsilica addition exhibit superior properties over the pure cement-based mortars upon carbonation. Carbonation of C-S-H (AFm/AFt) gel results in the formation of capillary pores between 10–50 nm, which outbalances the shielding effects of carbonates formed, leading to the enhanced photocatalytic properties. Moreover, C-S-H gel maintains its high NO_2 adsorption capacity even after carbonation, resulting in the high selectivity of the photocatalysis.

1. Introduction

Concrete is the most produced man-made material worldwide, and the consequent large concrete surfaces exposed to the solar irradiation provide an excellent opportunity for applying the photocatalytic oxidation (PCO) technology for air purification purpose, especially in the highly polluted urban areas. Incorporation of photocatalytic semiconductors into a concrete surface layer or as a surface coating induces the photocatalytic oxidation of air pollutants and in the meantime provides self-cleaning effects to the concrete [1,2]. Among available semiconductors, TiO_2-based photocatalysts are most commonly used and investigated due to their high photocatalytic efficiency, high stability and low price [3]. Since nitrogen oxides (NO_x) (the generic term for a group of highly reactive gases, including nitric oxide (NO) and nitrogen dioxide (NO_2)), cause a great concern on health and environment, in recent years, photocatalytically active materials for NO_x removal have been extensively investigated [4–7]. The photocatalytic conversion of NO with the use of TiO_2 photocatalyst can be described in a simplified way with the following reaction [8]:

$$NO_{(g)} \xrightarrow[Air+H_2O_{(g)}]{TiO_{2(s)}+h\nu} NO_{2(g)} \xrightarrow[Air+H_2O_{(g)}]{TiO_{2(s)}+h\nu} NO^-_{3\,(ads)}$$
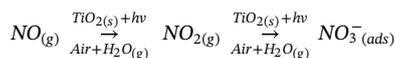
The pollutants degradation efficiency of photocatalytic concrete depends on the mix design and the production approach. The main parameters affecting the photocatalytic performance of concrete are the type of binder used (pH, phase composition), porosity, microstructure, surface roughness, colour of concrete, and type and dosage of photocatalyst [6,9–11].

The photocatalytic oxidation of pollutants is a superficial reaction, taking place on the concrete surface that is exposed to the atmospheric conditions, therefore, durability issues are of high significance. Among various durability aspects, carbonation is one of the most important aging-related factors. Upon carbonation, phase composition of concrete is altered and so the pH, specific surface area and porosity are also affected. Moreover, the overall titania content in the total volume of solids is reduced since the absorbed CO_2 reacts with the hydration products to form calcium carbonates. However, up till now the understanding of the carbonation effects on photocatalysis is very limited. Previous few studies implied that carbonation of the photocatalytic concrete causes the reduction of photocatalytic efficiency, possibly due to the shielding effects of carbonation products on titania particles and the reduction of porosity [12,13]. However, these assumptions can be only valid when Portland cement carbonation is considered. As widely described in the literature, the impact of carbonation on the concrete microstructure does not necessarily result in a porosity decrease e.g. when pozzolanic materials are added [14–16]. Moreover, it is not clear whether the changes in porosity or shielding effects are the governing factors causing the reduction of the photocatalytic performance. Even

---

more importantly, with the addition of pozzolanic materials, it is unknown whether the decrease of photocatalytic performance upon carbonation is actually observed. Up to now, no systematic study has been performed on this topic.

The microstructural changes in concrete upon carbonation depend on the CO_2 binding capacity and phase composition of concrete, with a particular impact of the quantity of portlandite. The reaction of CO_2 with portlandite leads to the formation of $CaCO_3$ and consequent structural densification. With the addition of pozzolanic material, the CO_2 binding capacity of concrete is reduced due to the lower overall CaO/SiO_2 ratio, and portlandite is consumed to form additional C-S-H gel. Thermodynamic modelling predicts that carbonation of C-S-H gel takes place after the carbonation of CH [15,17], whereas the experimental data show that carbonation of C-S-H and CH occurs simultaneously [14,18,19]. Carbonation mechanism of C-S-H gel differs from the carbonation of CH being governed by the decalcification of the C-S-H layers and formation of amorphous silica [20]. In consequence, the reduction of the volume of the solids (known as carbonation/decalcification shrinkage) and coarsening of the pores is often accompanied by the increase of the total concrete porosity upon carbonation of C-S-H gel. Morandeau et al. [21] showed that when a part of cement is substituted with class F fly ash, the formation of big capillary pores (> 50 nm) occurs during carbonation. Similarly, Shi et al. [15] reported an increased volume of the pores in the range between 10 and 100 nm for metakaolin and metakaolin/limestone mortars. It is worth mentioning that also for Portland cement mortars, even if the total amount of pores is reduced, coarsening of the pores is observed upon carbonation [14].

Considering the impact of carbonation-induced microstructural changes on the photocatalytic performance of concrete, it needs to be kept in mind that whereas porosity has a significant influence on the efficiency of the pollutants oxidation process, a higher porosity of concrete does not necessarily result in better photocatalytic properties [22,23]. Moreover, the strong presence of nanopores (< 50 nm) is found to negatively affect the photocatalytic properties [9,22]. Jimenez-Relinque et al. [9] suggested an optimum pore size range between 50 and 500 nm for the NO_x, and between 100 and 500 nm for the organic dyes degradation, while investigating 28 days hydrated mortars. However, it needs to be noticed that the inner porosity of mortars does not reflect the real surface porosity, where carbonation is unavoidable. Therefore, the re-evaluation of the impact of surface properties of mortars, affected by the mortars capacity to bind CO_2 and the carbonation mechanism, on the photocatalytic properties is required. Owing to the porosity increase when C-S-H gel carbonates and porosity decrease when portlandite carbonates, we hypothesize that from the microstructural point of view, photocatalytic properties can be optimized by controlling the changes in the pore structure of concrete surface upon carbonation, which are directly related to the initial mix design.

Another important aspect is the carbonation impact on the selectivity of the photocatalytic process. Even if the optimal properties of concrete for the photocatalytic oxidation are provided, the total outcome of air purification can be still very limited or even take a negative value [24]. This can be attributed to the insufficient conversion of air pollutants to final products, e.g. nitric oxide (NO) to nitrates or volatile organic pollutants to CO_2 and H_2O. During the photocatalytic oxidation of NO, firstly NO_2 is formed that is then oxidized to nitrates (NO_3^-). Instead of being further photocatalytically oxidized, part of the produced NO_2 can be potentially released to the atmosphere. Since the toxicity of NO_2 is significantly higher than NO [7], the ability of photocatalytic mortars for selective oxidation is an important feature, whereas only limited research can be found on this topic. Previous studies were mainly focused on the improvement of the photocatalytic reaction selectivity through the modification of the photocatalyst itself, which in turn often results in the reduction of the NO conversion [24,25]. At the same time, higher values of the selectivity are observed

when the photocatalyst is loaded into the cementitious matrix in comparison to pure photocatalysts [26]. Nevertheless, the understanding of this behavior remains limited and the effects of carbonation on the selectivity have never been thoroughly investigated.

The photocatalytic oxidation of NO_2 is only one of the possible routes for the NO_2 elimination. For example, Araña et al. [8] recently revealed that NO_2 abatement by a photocatalyst is not necessarily an effect of photocatalytic oxidation but rather of the adsorption of NO_2 on the photocatalyst surface, which later undergoes a disproportionation reaction as a prevalent mechanism for NO_2 elimination. Moreover, a few studies already indicated that the chemical composition of the hosting matrix, where photocatalyst is loaded, affects the NO_2 abatement [27,28]. Thus, providing a surface with a high NO_2 adsorption capacity could be a potential solution for the selectivity improvement. Taking into account the high NO_2 adsorption capacity of portlandite and C-S-H gel [29,30], the cementitious matrix seems to be an excellent substrate for photocatalytic processes. Nonetheless, the carbonation impact needs to be further evaluated since the ability of calcium carbonates to adsorb NO_2 is substantially lower than that of portlandite and C-S-H gel [31]. Furthermore, it is especially important to combine the effects of the formation of carbonates with lower NO_2 adsorption capacity with the accompanying structural changes in order to reveal the real impact of carbonation on the selectivity.

This study aims to explore the role of the carbonation mechanisms on the photocatalytic degradation of NO_x by cement mortars. The carbonation-induced physicochemical changes are analyzed and compared for two mortars series, the first one rich- and the second one free of portlandite. White cement is employed as the primary binder in both mortar series and pozzolanic microsilica is applied in the second mix to adjust the portlandite content. This strategy is used in order to differentiate between the impact of carbonation of CH and C-S-H phase on the photocatalytic performance, and in consequence, to propose a mix design optimization method in order to retain the photocatalytic efficiency during the service life of photocatalytic mortars. For a deeper understanding of the impact of the surface chemistry and microstructure on the selectivity of the photocatalytic processes, the capacity of un-carbonated and carbonated mortars to adsorb toxic NO_2 in darkness is analyzed in this study.

2. Experimental

2.1. Materials

CEM I 42.5 LA white cement (Aalborgportland), microsilica (Elkem 920ED) and standard sand were used in this study as the raw materials. In order to provide representative results, which are valid for different types of photocatalysts, three photocatalysts were selected and investigated, including commercially available Aeroxide TiO_2 P25 (Evonik Industries) consisting of 80% of anatase and 20% of rutile (specific surface area (SSA) ∼ 50 m²/g), KRONOclean 7000 carbon-doped titania (SSA ∼ 251 m²/g) (Kronos International), and one home-synthesized composite photocatalyst consisting of 85% of SiO_2 and 15% of TiO_2 (SSA ∼ 200 m²/g) prepared with a sol-gel method (more detailed synthesis information is presented elsewhere [32]). The P25 and KRONOclean 7000 (Kronos) TiO_2 were used as reference photocatalysts, the first one being photocatalytically active only under UV irradiation and the second one with the photo-response extended to the visible regions. To the homemade composite, the coating of titania over silica nanoparticles was applied with the aim to increase the specific surface area of the photocatalyst and in the meantime to improve its mechanical properties and thermal stability [33]. Furthermore, the photocatalytic activity of silica-titania composite over pure titania could be enhanced due to: i) the ability of silica for long-term adsorption of the pollutant molecules, ii) high redox potential of the electrons and holes, iii) additional scattering of the light to the titania surface [34]. The efficiency of the applied coating method was examined by the
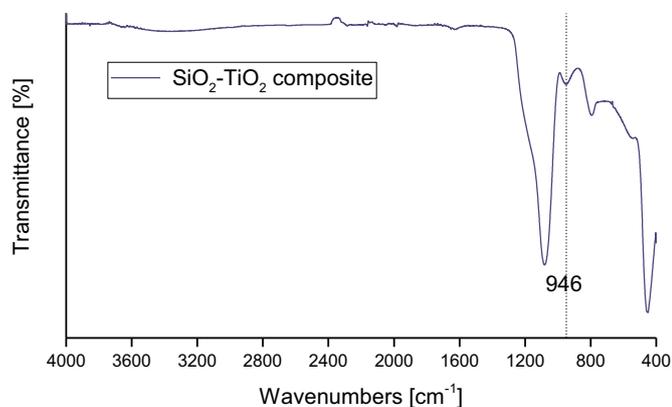
Fig. 1. FTIR spectrum of silica- titania composite.

FTIR measurement (Fig. 1). The band located at 946 [cm^{-1}] corresponds to the vibration of Si-O-Ti, confirming the formation of the inorganic network between SiO_2 and TiO_2 [35–37].

2.2. Methodology

2.2.1. Mix design

Two series of standard mortars with the water to binder ratio (w/b) of 0.5 were prepared and tested in this study. The first series consisted of white cement-based mortars while in the second series, 30 wt% of cement was replaced with microsilica. For each composition, three photocatalysts were investigated, keeping the amount of photocatalyst at a constant level of 5 wt% of the binder. Superplasticizer MasterGlenium® 51 was used to adjust the consistency of the mixtures. The mix design of the mortars is described in Table 1.

2.2.2. Mortars manufacture

Cement and microsilica were firstly intermilled in a planetary ball mill (Pulverisette 5, Fritsch). Milling was employed in this study in order to ensure a proper homogeneity of the binder, which nevertheless would unavoidably cause slight alteration of the specific surface area of cement and microsilica. Subsequently, the photocatalysts were dispersed in 200 ml of water with an ultrasonic device (Hielscher UP400S) for 10 min (amplitude of 75%). An ice water bath was used to prevent heating of the solutions. Before mixing with cement (cement and microsilica) and sand, the temperature of the solutions was controlled and kept constant at 21 ± 1 °C. Mixing of the mortars was performed in accordance with EN 196-1:2005 standard. The amounts of superplasticizer were adjusted to provide similar workability of the mortars, falling in S4 class according to EN 206-1 standard. The mortars were cast into $10 \times 20 \times 2 \, cm^3$ molds, vibrated for 1 min and covered with plastic sheets to prevent the moisture loss and carbonation. After 24 h, all mortars were demolded, sealed with self-adhesive aluminum foil, placed in the humidity chamber (RH > 95%, 20 °C) and cured for 5 months to ensure sufficient hydration. At the end of the curing period, the samples were cut in half with a saw, to create plates with a thickness of about 1 cm. This procedure was applied in order to provide surfaces

with the same roughness, to eliminate wall effects and to avoid the eventual early age carbonation during casting and demolding of the samples. As water treatment during the cutting could not be avoided, and the photocatalytic efficiency is strongly influenced by the moisture level, after cutting, the samples were immediately inserted and dried in a nitrogen chamber to limit the carbonation.

2.2.3. Scanning Electron Microscopy + Energy Dispersive X-ray Spectroscopy (SEM + EDX)

For Scanning Electron Microscopy (SEM) investigations, hydration of mortars was stopped by immersing the samples in isopropanol for 3 days and subsequent drying in an oven at 40 °C. The extracted mortar specimens were epoxy-impregnated, ground and polished with a series of successively finer grades of alumina powders. Polished sections were sputtered with gold by using an Emitech K550X sputter coater (current 65 mA, coating time 20 s). Phenom ProX scanning electron microscope with an accelerating voltage of 15 kV was used to perform images. Mapping analysis was conducted with the Element Identification (EID) software package with fully integrated Energy Dispersive Spectrometer (EDS).

2.2.4. Accelerated carbonation and phenolphthalein test

The 5 months old mortars were exposed to CO_2 atmosphere for 28 days in a carbonation chamber. The conditions of 3% CO_2 and RH = 65% were selected in order to facilitate the formation of carbonates, preserve the nanostructure of C-S-H and at the same time to mimic the natural carbonation process [19,38]. Phenolphthalein test was used to determine the carbonation depth in the samples at the end of the carbonation period. The mortar plates were split with a saw and the carbonation profiles were obtained by spraying the cross-sections with a 1 wt% phenolphthalein aqueous solution.

2.2.5. Mercury intrusion porosimetry and thermogravimetry

For mercury intrusion porosimetry (MIP) measurements, 3 mm thick surface plates were cut from the un-carbonated and carbonated mortars. The plates were subsequently split with the tongs into cubic pieces, immersed in isopropanol for 7 days and dried in a desiccator for another 7 days. The AutoPore IV Series Mercury Porosimeter (Micromeritics), working with a pressure between 14 kPa and 228 MPa, was used for the measurements. The surface tension of mercury (γ_{Hg}) was 485 N/m and a contact angle (θ) of 130° was applied [39].

The remaining parts from the surface plates were powdered in a planetary ball mill (Pulverisette 5, Fritsch). About 50 mg of powders were thermally treated using a Jupiter STA 449 F1 Netzsch instrument. The samples were heated up from 40 to 1000 °C at the rate of 5 °C/min using nitrogen as the carrier gas.

2.2.6. Photocatalytic efficiency assessment

The photocatalytic oxidation (PCO) experiments were carried out in accordance with ISO 22197-1:2016 standard, using a plug-flow setup (Fig. 2). Nitric oxide (NO) was employed as a model pollutant. The mortars were tested before and after the accelerated carbonation.

The mortars were firstly assembled in the reactor and the position of the samples was adjusted to create a 3 mm gap between the sample surface and the top of the reactor. The reactor was covered in order to

Table 1
Mix design of the photocatalytic mortars.

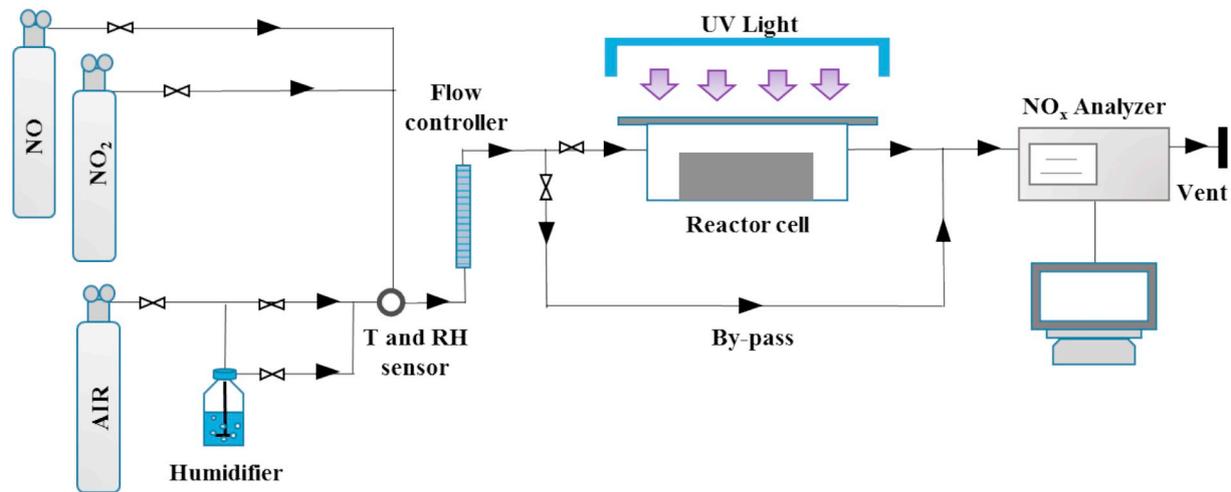|		Cement [g]	Microsilica [g]	Sand [g]	TiO$_2$ P25 [g]	KRONO-clean [g]	TiO$_2$-SiO$_2$ [g]	w/b	SP dosage [%]
White cement	P25	450	–	1350	22.5			0.5	0.4
	Kronos	450	–	1350		22.5		0.5	0.4
	SiO$_2$-TiO$_2$	450	–	1350			22.5	0.5	0.4
White cement	P25	270	180	1350	22.5			0.5	1.2
+ microsilica	Kronos	270	180	1350		22.5		0.5	1.2
	SiO$_2$-TiO$_2$	270	180	1350			22.5	0.5	1.2

Fig. 2. The scheme of the PCO experimental set-up.

Table 2
PCO experimental conditions.

Parameter	Value	Unit
Relative humidity	50	%
Initial NO concentration	1	ppm
Volumetric flow rate	3	L/min
Light intensity (UVA)	10	[W/m^2]

prevent the uncontrolled degradation of pollutants while adjusting the measurements parameters. All the measurements were performed under stable conditions, described in Table 2. The desired concentration of NO pollutant was achieved by mixing the NO with the synthetic air. Firstly, the gas was allowed to flow through a by-pass until the stabilized values of the light radiation, NO concentration and humidity were reached. Afterwards, the gas flow was switched from the by-pass to the reactor and the data acquisition was started. During the first 15 min of the measurements, the reactor was kept covered in order to ensure stable conditions. Subsequently, the samples were illuminated through the glass plate for 1 h, when steady-state condition was reached. The APNA-370 (Horiba) analyzer was used to monitor the concentration of the pollutants.

Taking into account the eventual NO$_2$ release, the photocatalytic efficiency of the designed materials was characterized by the NO$_x$ (NO + NO$_2$) conversion and calculated according to

$$\%Convertion = \frac{[c_{NO_x}]_{in} - [c_{NO_x}]_{out}}{[c_{NO_x}]_{in}} \times 100\% \tag{1}$$

where $[c_{NO_x}]_{in}$ is the average initial concentration [ppm] of the first 5 min before turning on the light; $[c_{NO_x}]_{out}$ is the average outlet concentration [ppm] of the last 5 min of the irradiation period.

The selectivity of photocatalytic reaction towards the formation of nitrates S(%) [24,28] was calculated with the following formula

$$S\% = \frac{[c_{NO_x}]_{in} - [c_{NO_x}]_{out}}{[c_{NO}]_{in} - [c_{NO}]_{out}} \times 100\% \tag{2}$$

In order to evaluate how the selectivity of NO to NO$_2$ is influenced by the cementitious matrix, adsorption of NO$_2$ on the surface of he mortars was also measured with the PCO setup. Tests were performed in darkness by flowing a mixture of synthetic gas and 0.5 ppm of NO$_2$ through the reactor. The measurement time, humidity, and gas flow were kept identical as for the PCO measurement.

3. Results analysis

3.1. Mortars characterization

3.1.1. EDX mapping analysis

In highly alkaline cement environment, titania nanoparticles tend to agglomerate [40], while providing a homogenous dispersion of photocatalyst in the cementitious matrix is crucial to ensure the high effective surface area of the photocatalyst for the air purifying reactions to occur and to eliminate the statistical error of the measurements of photocatalytic oxidation caused by the local agglomeration of titania particles. This was therefore addressed in this study by applying the ultrasonic treatment (see Section 2.2.2). The dispersibility of the photocatalysts in cement mortars was examined with EDX mapping analysis. It can be seen from Fig. 3 that satisfying dispersion of titania was achieved. The homemade silica-titania photocatalyst was characterized by a larger size variability compared to P25 (Fig. 3b vs. Fig. 3a), which was caused by agglomerates with the size up to ~10 μm formed during the manufacture of the composite. Nevertheless, the overall distribution of the composite in the mortars was homogenous. The homogenous dispersion of the different types of photocatalysts contributed to the maximization of their potential in terms of air pollutant removal efficiency.

3.1.2. Thermogravimetric analysis & phenolphthalein test

Fig. 4 shows the differential thermogravimetric (DTG) profiles of mortars before and after the accelerated carbonation treatment. The thermogravimetric (TG) data were collected from the powdered 3 mm upper layers of mortar plates. After 5 months of hydration, two main mass losses were observed in pure cement-based samples due to the release of water from C-S-H (AFt/AFm) phases (30–300 °C) and portlandite (400–450 °C), whereas no portlandite was observed in the mortars with microsilica addition. The successful elimination of portlandite in mortars with microsilica enables differentiation between carbonation of C–S–H (AFt/AFm)/ CH (white cement mortars) and C–S–H (AFt/AFm) (white cement + microsilica mortars) in this study.

After 28 days' treatment in the carbonation chamber (3% CO$_2$), samples revealed an additional mass loss at the temperature range between 600 and 800 °C in pure cement-based mortars, and a broad peak between 300 and 700 °C in the mortars with microsilica addition. These two new peaks are assigned to the decomposition of calcium carbonates. It is evident that the carbonation products of C–S–H gel and AFt/ AFm decompose at significantly lower temperatures than the carbonates in CH abundant mortars. Decomposition of carbonates at lower temperature ranges in mortars with the addition of pozzolanic material
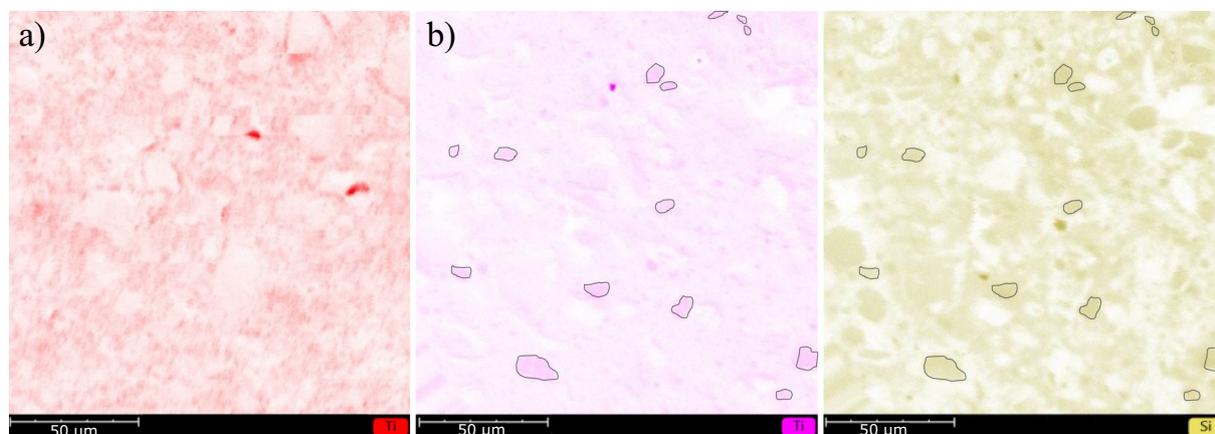
Fig. 3. EDX mapping showing the distribution of a) titanium in the cement mortar with the P25 addition and b) titanium (in pink) and silicon (in gold) in the cement mortar with the silica-titania composite addition (selected areas represent silica-titania agglomerates formed during the manufacture of photocatalyst). (For interpretation of the references to colour in this figure legend, the reader is referred to the web version of this article.)

has been reported in previous studies [14,15], and this is attributed to the formation of amorphous/poorly crystalline carbonates [41,42]. It should be mentioned that whereas portlandite carbonates mostly to calcite [38], carbonation of C-S-H gel leads also to the formation of vaterite [38,43], which decomposes at lower temperatures than calcite even in the crystalline form [44]. Sevelsted et al. [20] showed with the $^{13}C\{^1H\}$ CP/MAS NMR that in a hydrous environment, the formation of calcium carbonate hydrates can also take place. Thermal decomposition of these compounds occurs between 400 and 500 °C [45].

Different mechanisms of carbonation in mortars rich and lean of portlandite led to the substantial differences in the carbonation extents. Comparison between the phenolphthalein profiles of carbonated samples and amounts of carbonates formed in both systems clearly indicates that pure cement mortars are more resistant to the carbonation than mortars with the microsilica addition. In the cement mortars, crystalline carbonates are formed, whereas in mortars with the pozzolanic material predominance of amorphous/poorly crystalline carbonates is observed.

3.1.3. Porosity and pore size distribution

The microstructure of the mortars surface layer (3 mm), which was altered by the carbonation, was investigated via Mercury Intrusion Porosimetry. The cumulative porosity results (Fig. 5) revealed that carbonation of portlandite and C–S–H led to a decrease in the total porosity of the pure cement mortars surface, whereas an increase in the

total porosity was observed in the mortars with microsilica addition. These findings are in agreement with the observations made in the previous studies on the carbonation of mortars with SCMs [14,15], and it is worth noting that the addition of photocatalysts did not alter the pore structure evolution beyond carbonation. In the cement based mortars changes in the total porosity were substantially lower than that in microsilica mortars which correlates well with the lower carbonation extent in cement mortars as described with DTG and phenolphthalein test data. Changes in the total porosity between the samples with different photocatalysts can be explained by slight differences in mortars consistency.

The changes in the pore size distribution for both mortar series during the carbonation are presented in Fig. 6. For pure cement-based mortars, a clear decrease of the number of capillary pores between the 10 and 50 nm, accompanied by slight coarsening of the pores, was observed upon carbonation process. Mortars with microsilica addition initially contained higher amounts of pores below 10 nm, after carbonation, however, the number of capillary pores between 10 and 50 nm drastically increased. Coarsening of the pores during the carbonation of mortars with SCMs was also reported elsewhere [14,15,46], and can be explained by the so-called "decalcification shrinkage". Decalcification shrinkage is particularly visible for C-S-H gels with Ca/Si ratios below 1.2, as reported in the study of Chen et al. [47] where, similar to our system, the paste containing 70% of white cement and 30% of microsilica was investigated. The appearance of bigger pores of ~1 μm in
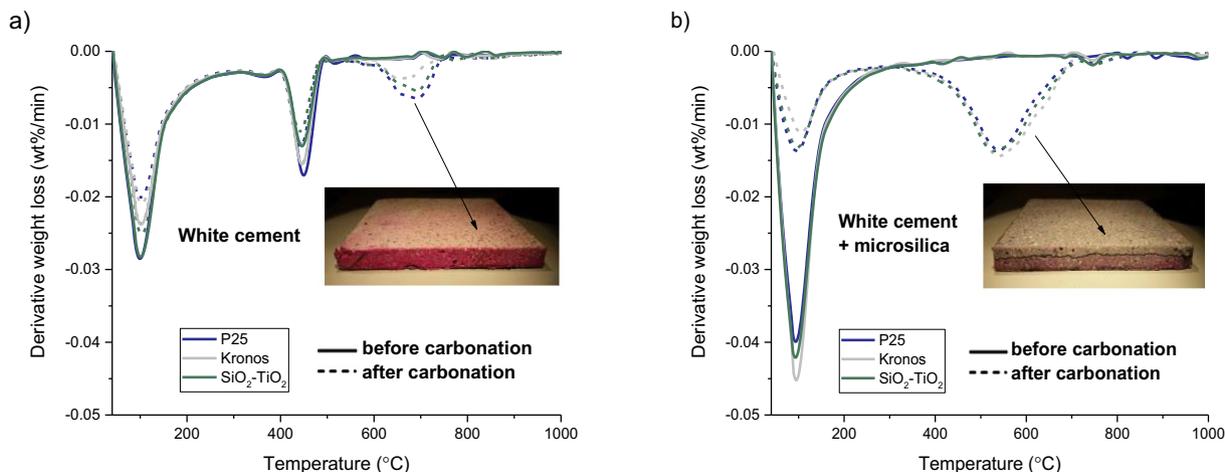
Fig. 4. DTG curves of carbonated (dash line) and non-carbonated (solid line) a) white cement, b) white cement + microsilica mortars. The carbonation depths measured with phenolphthalein test are representatively visualized regardless of the type of titania used.
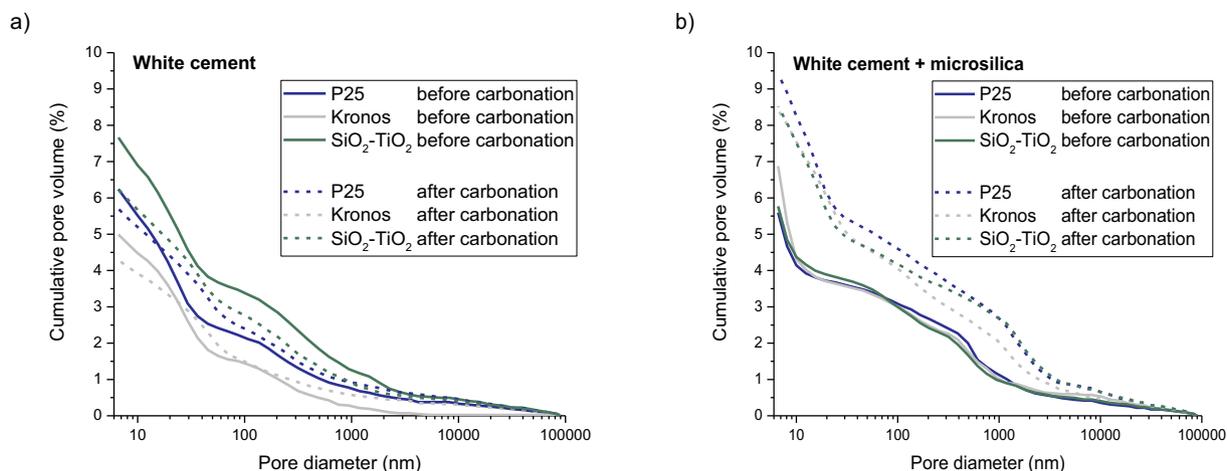
a)   b)

Fig. 5. Cumulative pore volume derived from Mercury Intrusion Porosimetry of a) white cement mortars and b) white cement + microsilica mortars, before and after accelerated carbonation.

microsilica mortars can be assigned to the formation of cracks during the carbonation of C-S-H gel. Formation of cracks upon C-S-H gel carbonation is found to occur in both accelerated and natural conditions [38].

3.1.4. SEM analysis

The microscopic observations of the surface of the mortars after accelerated carbonation treatment (Fig. 7) showed that carbonation of white cement hydration products led to the formation of a dense layer of carbonate crystals, strongly affecting the effective exposure of photocatalyst (Fig. 7a). In contrast, in mortars with microsilica addition (Fig. 7b), only a limited formation of crystalline carbonates was observed and the gel-like structure of C-S-H phase was preserved. Additionally, in agreement with the porosity results, the formation of cracks was observed in microsilica mortars.

3.2. Photocatalytic efficiency

3.2.1. NOx oxidation rate

The efficiency of photocatalytic oxidation of NO_x before and after carbonation is presented in Fig. 8. Comparison of the results obtained for pure cement-based mortar and microsilica mortars clearly reveals that both, photocatalyst type and matrix composition/microstructure strongly influence the photocatalytic performance. In regard to the photocatalytic oxidation rate, in un-carbonated white cement mortars, the best performance was observed for P25, followed by the SiO_2-TiO_2

composite and Kronos. Furthermore, the photocatalytic efficiency of the mortars with SiO_2-TiO_2 composite was the most sensitive to the surface changes upon carbonation. As SiO_2-TiO_2 composite formed agglomerates (as shown with EDX mapping, see Section 3.1.1), it is apparent that due to the microstructural changes there was a limited exposure of SiO_2-TiO_2 composite for the photocatalytic reaction.

It is worth mentioning that the photocatalytic oxidation rates of cement mortars before the carbonation were similar to those observed in other studies [9,10]. Upon carbonation, a decrease of photocatalytic performance was observed in all pure cement mortars and increase in all microsilica containing mortars, following the observed microstructural changes. This behavior will be discussed later in this paper.

3.2.2. Selectivity

The selectivity of the photocatalytic oxidation of NO, which accounts for the formation and release of NO_2, is presented in Fig. 9. The selectivity of photocatalytic conversion observed in this study for the mortars before the carbonation (up to 97%) is higher than that observed e.g. by Yang et al. [26], where similar formulation of the mortar was used. This can be an effect of differences in the porosity [11], dispersion of titania in the mortar matrix and strong carbonation impact which is unavoidable during the standard curing of the samples. These effects are later discussed in this study. Among the investigated photocatalysts, silica-titania composite revealed the highest selectivity, followed by carbon-doped Kronos titania and titania P25 as the least effective photocatalyst, regardless of the carbonation stage. The
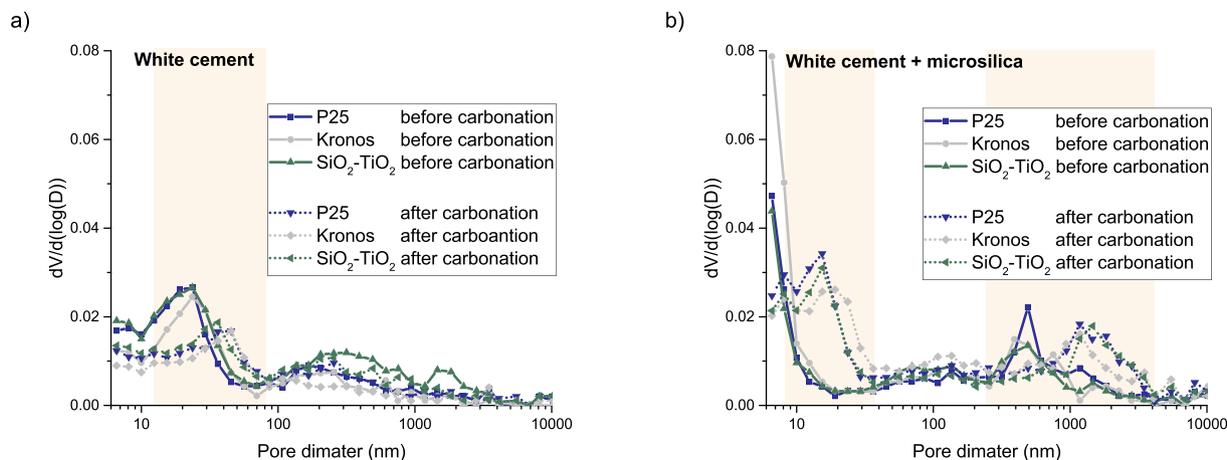
a)   b)

Fig. 6. Differential pore size distribution in a) white cement mortars and b) white cement + microsilica mortars before and after carbonation.

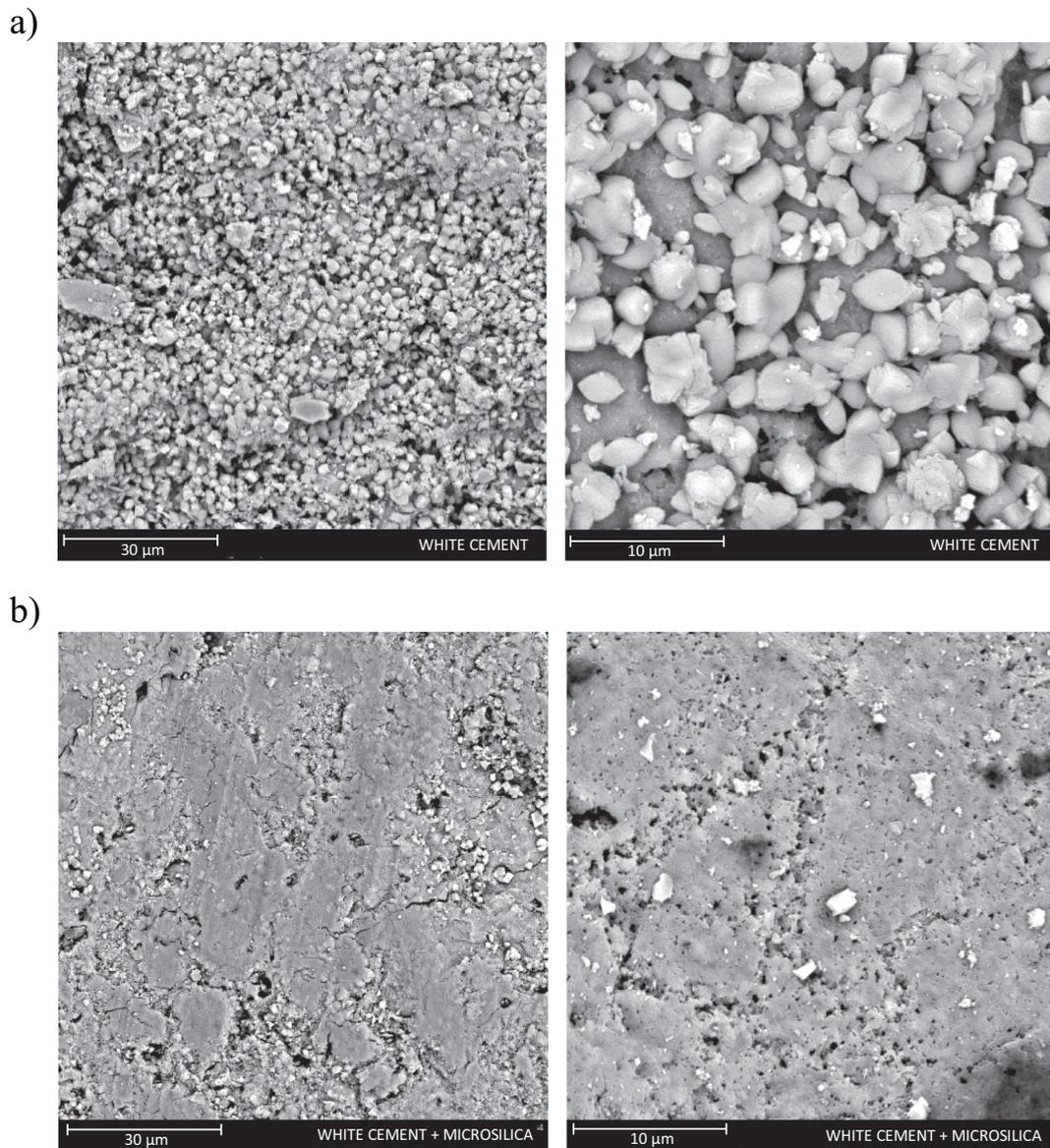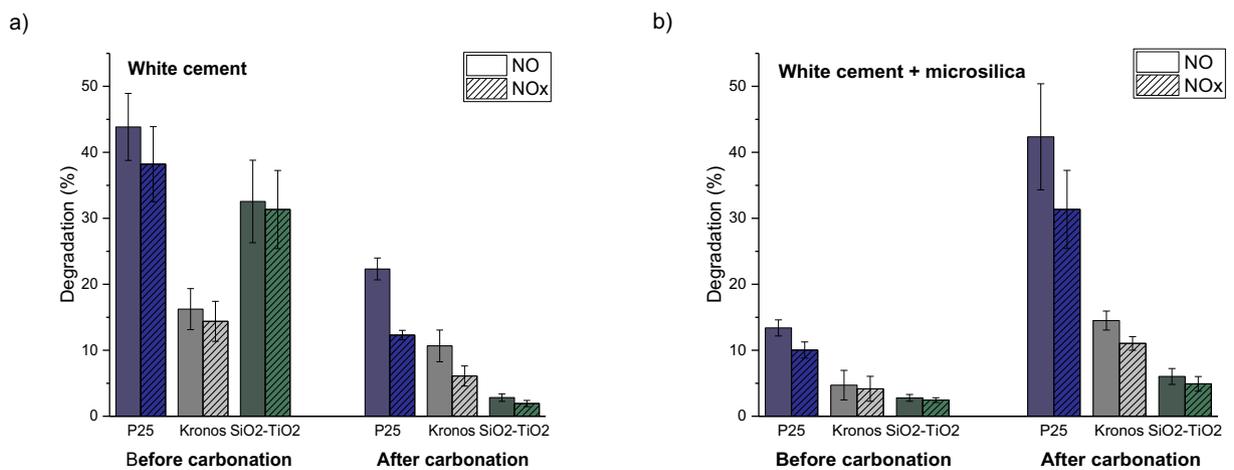**Fig. 7.** SEM images of a) pure cement mortars surface and b) microsilica mortars surface after carbonation.

Fig. 8. The NO and NO$_x$ degradation by photocatalytic a) white cement mortars and b) white cement + microsilica mortars before and after carbonation.
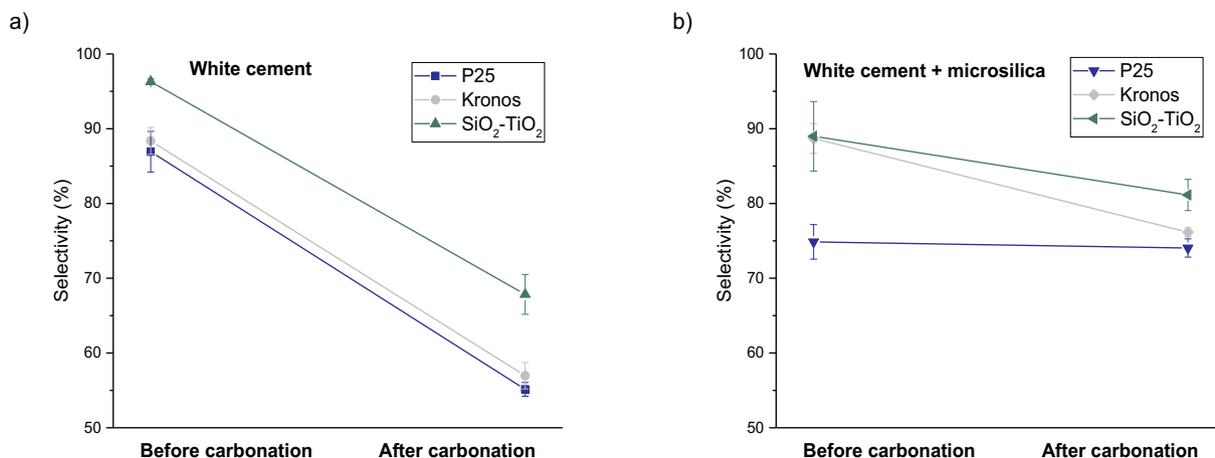
a)

b)

Fig. 9. Photocatalytic selectivity of a) white cement mortar and b) white cement + microsilica mortars before and after accelerated carbonation.

superior performance of silica-titania composite and Kronos titania over P25 can be a result of around 4 times higher specific surface area of these photocatalysts. A higher specific surface area results in a higher NO_2 adsorption capacity of the photocatalyst, which is a crucial factor if one considers that NO_2 can be not only further photocatalytically converted but also be adsorbed on the surface and e.g. undergoes disproportionation, as shown by Arana et al. [8]. Additionally, silica-titania composite offers extra hydroxyl groups on the surface and enhanced hydrophilic properties [34]. Even though in the study of Hakki et al. [48] it was shown that Ti-O-Si binding negatively affects the nitrate selectivity, the abovementioned features seem to outbalance this effect. After carbonation, the selectivity of the samples dropped significantly for pure cement-based mortars, whereas only a slight drop was observed for microsilica mortars.

3.2.3. NO_2 adsorption

The adsorption of NO_2 gas on the surface of the mortars was investigated in darkness following the experimental scheme of PCO test, before and after carbonation. The results shown in Fig. 10 express that the highest adsorption capacity was observed for mortars with microsilica addition. Furthermore, microsilica mortars maintained their high adsorption capacity even after carbonation. In contrast, a drastic drop of NO_2 adsorption capacity was observed for pure cement-based mortars after carbonation - the measured values were only slightly higher than for borosilicate glass which was used as a reference.
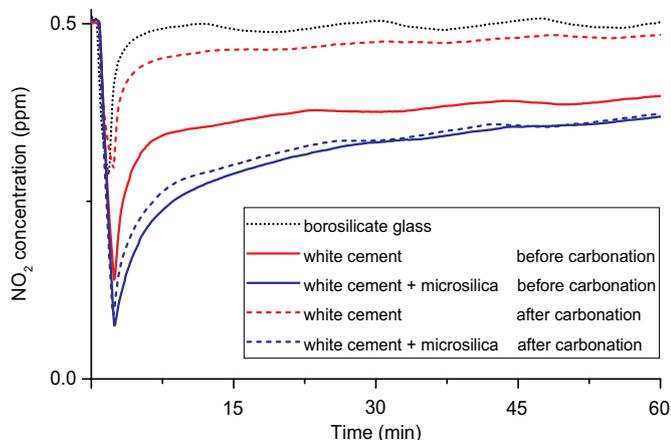

Fig. 10. Adsorption of NO_2 on the mortars performed in the darkness before and after accelerated carbonation.

4. Discussion

4.1. Influence of carbonation on photocatalytic performance

The comparison between the photocatalytic response of mortars with and without microsilica addition, and three types of photocatalysts used, enabled determination of the main parameters affecting the photocatalytic performance of mortars upon carbonation. The highest photocatalytic activity was observed for pure cement-based mortars before carbonation. This could be assigned to the presence of capillary pores in the range between 10 and 50 nm since for microsilica mortars, with the prevalence of pores below 10 nm, the NO oxidation rates were about 3 times lower. The predominant role of porosity was further confirmed by the analysis of the microsilica mortars, where as a result of C-S-H (AFt/AFm) phase carbonation, an increase of photocatalytic activity was observed. The improved photocatalytic activity coincided with the occurrence of capillary porosity between 10 and 50 nm. Therefore, it can be concluded that the microstructural changes caused by C-S-H (AFt/AFm) carbonation boost the photocatalytic activity due to the formation of capillary pores in the range between 10 and 50 nm, which can outbalance any shielding effects of the carbonates formed (as revealed with the thermogravimetric analysis and phenolphthalein test). In contrast, in the cement mortars series, with high portlandite content, the drop of photocatalytic activity, observed upon carbonation was a result of both structural densification and formation of a dense layer of crystalline carbonates, as revealed with SEM analysis. Moreover, shielding effects of the hydration and carbonation products, limiting the TiO_2 exposure on the surface, were substantially stronger when photocatalyst was loaded in the form of agglomerates. Whereas the photocatalytic efficiency of cement mortars with P25 and Kronos titania addition dropped about 1.5–2 times upon carbonation, in mortars with SiO_2-TiO_2 composite agglomerates, the photocatalytic performance was reduced > 10 times.

The impact of capillary pores between 10 and 50 nm on the photocatalytic properties of mortars observed in this study argues with the previous findings on the influence of porosity on the photocatalytic performance. Contradictory to the optimum porosity ranges for pollutants oxidation presented e.g. by Rimenez-Relinque et al. [9] between 50 and 500 nm, we have found that the presence of pores in the size range between 10 and 50 nm in the surface of the mortars can significantly boost the photocatalytic efficiency. It is shown that capillary porosity in the range between 10 and 50 nm provides satisfying photocatalytic properties to cementitious mortars and that the elimination of portlandite enables to avoid the drop of the photocatalytic properties upon carbonation.
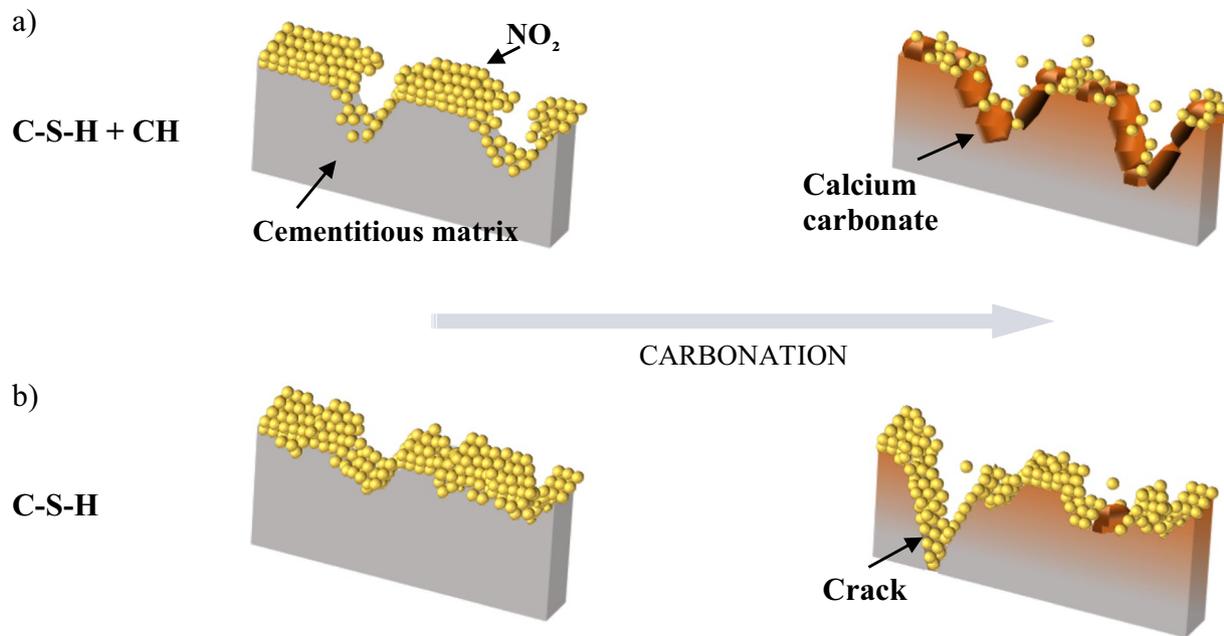
Fig. 11. Conceptual model of the adsorption of NO_2 on the surface of mortars a) based on pure cement and b) with microsilica addition, before and after carbonation process.

4.2. Influence of carbonation on selectivity

The release of NO_2 to air is not desired since NO_2 is more harmful than NO [49]. Therefore, the selectivity of the photocatalytic reaction towards the elimination of intermediate NO_2 is one of the main issues in the practical application of photocatalytic technology to deal with NO removal. During the photocatalytic process, NO_2 can be further photocatalytically oxidized [50], decomposed via photolysis [4] or be just adsorbed on the surface and e.g. eliminated via disproportionation [8]. The latter route is pH-dependent and therefore, the impact of carbonation becomes crucial. The observed drop of selectivity after the reduction of pH of mortars surface upon carbonation could be partially explained with this route, however, further investigation is needed. This study shows that the amount of the NO_2 released during the photocatalytic experiments depends not only on the photocatalyst itself (as described in Section 3.2.2) but also on the changes of the cementitious matrix upon carbonation. Before carbonation, the selectivity of the photocatalytic reaction was very high for pure cement-based mortars. Similarly, microsilica mortars revealed high selectivity before carbonation, except the sample with P25 photocatalyst. The lower selectivity of this mortar can be related to the significantly lower specific surface area of the P25 photocatalyst, which in combination with low porosity of mortars is insufficient to capture the NO_2 when relatively higher amounts of NO are photocatalytically oxidized. For carbonated samples, the drastic drop was observed when portlandite reacted with CO_2 forming a 'protective' layer of carbonates on the surface and the selectivity was maintained or only slightly reduced for microsilica samples, even though their photocatalytic efficiency increased significantly after carbonation.

On the other hand, the study on the NO_2 adsorption capacity of the mortars in darkness revealed superior properties of microsilica samples over cement samples. In the darkness, only two routes for NO_2 abatement are possible - physical or chemical adsorption. The higher NO_2 adsorption capacity of microsilica mortars over cement mortars could be related to the higher specific surface area of the C-S-H gel compared to the surface area of large portlandite crystals. After carbonation, even though the drop of pH was observed (as shown with phenolphthalein test) on the surface of both sets of mortars, microsilica mortars maintained their high adsorption capacity. In the study of Thomas et al.

[51], it was revealed that specific surface area of C-S-H gel can be even doubled upon carbonation, as measured by nitrogen gas sorption and small-angle neutron scattering. Therefore, it is suggested that the drop in pH was compensated in this case with the higher specific surface area and porosity of the gel. In contrast, a significant decrease in the NO_2 adsorption capacity of cement mortars after carbonation was a result of the formation on the surface of a dense layer of carbonate crystals which are found to have a lower capacity to adsorb the pollutants [31]. Following the above discussion, a conceptual description of the adsorption of NO_2 on the surface of the mortars is proposed, as shown in Fig. 11, underlining the high NO_2 adsorption capacity of microsilica mortars after carbonation, where shielding effects are very limited and the effective surface area is maintained or even increased upon carbonation due to the changes in gel porosity and cracks formation.

It is therefore proposed that the cementitious matrix supports NO_2 elimination due to its high NO_2 adsorption capacity related to the high pH and specific surface area of the hydration products. The C-S-H gel is more favorable over portlandite, being able to maintain its high NO_2 adsorption capacity even after carbonation. Furthermore, with low oxidation rates, the ability of the cementitious products/photocatalysts to adsorb NO_2 is the main selectivity controlling factor, whereas with high pollutants oxidation rates, porosity starts to play a dominant role. The capillary porosity in the range between 10 and 50 nm is shown to increase the selectivity of the photocatalytic reaction. The positive role of open porosity on the NO_2 capture is in agreement with the observations made by Gauvin et al. [11]. This study shows that capillary porosity supports the NO_2 adsorption, presumably due to the overlong presence of NO_2 close to the sample surface rather than being immediately departed. It is postulated that with lower flows than applied in this study (3 l/min) the overall selectivity towards the elimination of NO_2 would be even higher. The negative influence of high flow rate and high concentration of the pollutants have been reported in several studies [26,52]. Despite the suboptimal experimental conditions applied in this study, the selectivity values were much higher than those observed for pure photocatalysts [24,28].

5. Conclusions

The impact of carbonation mechanism on the NO_x removal

Table 3
Carbonation impact on the NO$_x$ oxidation rate by photocatalytic mortars.

	Porosity 10 – 50 nm	Specific surface area[a]	TiO$_2$ exposure	NO$_2$ adsorption capacity	NO$_x$ oxidation rate after carbonation
CH + C-S-H (cement mortars)	High	High	High	High	Low
Carbonation impact	↘	↘	↘	↘	
C-S-H (cement + microsilica mortars)	Low	High	High	High	High
Carbonation impact	↗	↗	→	→	

[a] Predicted based on the available literature [51,53].

efficiency by cement mortars applying heterogeneous photocatalysis was investigated and the underlying roles of carbonation of portlandite and C-S-H gel were evaluated in this study. Pore structure, morphology, and phase composition of the designed mortars were studied. Photocatalytic oxidation efficiency of NO and the related selectivity were determined. Table 3 presents the summarized influence of the carbonation on the properties of mortars and their effect on the photocatalytic performance. The present study shows that the photocatalytic properties can be controlled and optimized with the initial mix design of the mortars concerning the influence of carbonation on the mortars microstructure. Pure cement is not recommended to be used as a matrix for photocatalysts, and instead, the addition of pozzolanic material is suggested. Here, microsilica was chosen as a pozzolanic material.

The following detailed conclusions are reached by the acquired results:

- Carbonation of portlandite leads to the structural densification of the mortar in the porosity range between 10 and 50 nm, and to the formation of the layer of crystal carbonates on the surface, limiting the exposure of TiO$_2$. In consequence, a drastic decrease of photocatalytic oxidation was observed for white cement mortars. Additionally, the agglomeration of the photocatalyst escalated the negative impact of the shielding effects and microstructural changes on the photocatalytic activity of mortars upon carbonation.
- Decalcification of C-S-H (AFm/AFt) gel in mortars with the addition of pozzolanic material results in the formation of capillary pores in the size range of 10 to 50 nm and increase of photocatalytic efficiency, indicating dominant effects of porosity restructuring on the photocatalytic performance over the shielding effects caused by the carbonation products, when C-S-H gel carbonates.
- The selectivity of photocatalytic processes depends on the type of the TiO$_2$ photocatalyst and the matrix properties. The highest selectivity was observed for the silica supported composite and was found to be affected by the specific surface area of the photocatalyst. The cementitious matrix can support the elimination of NO$_2$ due to its high ability to adsorb NO$_2$, associated with the high pH and specific surface area.
- The reduction of the mortars selectivity upon carbonation is minimized for mortars with microsilica addition where mainly C-S-H (AFm/AFt) gel carbonates. The superior impact of the C-S-H gel on the overall reaction selectivity is mainly related to the high specific surface area before and after carbonation and therefore, high capacity to adsorb NO$_2$.
- High pH together with the high specific surface area of the hydration products favor the NO$_2$ elimination and control the selectivity level when low oxidation rates of NO are observed. With higher oxidation rates, cementitious matrix supports the NO$_2$ elimination, however, the presence of porosity becomes a limiting factor - high capillary porosity improves the overall selectivity of the photocatalytic process possibly due to the prolonged residence time.

Declaration of Competing Interest

The authors declare that they have no known competing financial

interests or personal relationships that could have appeared to influence the work reported in this paper.

References

[1] A. Fujishima, K. Honda, Electrochemical photolysis of water at a semiconductor electrode, Nature 238 (5358) (1972) 37–38.
[2] A. Fujishima, X. Zhang, D.A. Tryk, Heterogeneous photocatalysis: from water photolysis to applications in environmental cleanup, Int. J. Hydrog. Energy 32 (14) (2007) 2664–2672.
[3] Q.L. Yu, H.J.H. Brouwers, Indoor air purification using heterogeneous photocatalytic oxidation. Part I: experimental study, Appl. Catal. B Environ. 92 (3–4) (2009) 454–461.
[4] M.M. Ballari, Q.L. Yu, H.J.H. Brouwers, Experimental study of the NO and NO2 degradation by photocatalytically active concrete, Catal. Today 161 (1) (2011) 175–180.
[5] M. Hunger, G. Hüsken, H.J.H. Brouwers, Photocatalytic degradation of air pollutants — from modeling to large scale application, Cem. Concr. Res. 40 (2) (2010) 313–320.
[6] C.S. Poon, E. Cheung, NO removal efficiency of photocatalytic paving blocks prepared with recycled materials, Constr. Build. Mater. 21 (8) (2007) 1746–1753.
[7] L. Yang, A. Hakki, F. Wang, D.E. Macphee, Different roles of water in photocatalytic DeNOx mechanisms on TiO 2: basis for engineering nitrate selectivity? Appl. Mater. Interfaces 9 (20) (2017) 17034–17041.
[8] J. Araña, D. Garzón Sousa, O. González Díaz, E. Pulido Melián, J.M. Doña Rodríguez, Effect of NO2 and NO3-/HNO3 adsorption on no photocatalytic conversion, Appl. Catal. B Environ. 244 (2) (2019) 660–670.
[9] E. Jimenez-Relinque, J.R. Rodriguez-Garcia, Characteristics and efficiency of photocatalytic cementitious materials: type of binder, roughness and microstructure, Cem. Concr. Res. 71 (2015) 124–131.
[10] M. Pérez-Nicolás, et al., Photocatalytic NOx abatement by calcium aluminate cements modified with TiO2: improved NO2 conversion, Cem. Concr. Res. 70 (2) (2015) 67–76.
[11] F. Gauvin, V. Caprai, Q.L. Yu, H.J.H. Brouwers, Effect of the morphology and pore structure of porous building materials on photocatalytic oxidation of air pollutants, Appl. Catal. B Environ. 227 (February) (2018) 123–131.
[12] M. Lackhoff, X. Prieto, N. Nestle, F. Dehn, R. Niessner, Photocatalytic activity of semiconductor-modified cement - influence of semiconductor type and cement ageing, Appl. Catal. B Environ. 43 (3) (2003) 205–216.
[13] M.V. Diamanti, F. Lollini, M.P. Pedeferri, L. Bertolini, Mutual interactions between carbonation and titanium dioxide photoactivity in concrete, Build. Environ. 62 (2013) 174–181.
[14] V. Shah, K. Scrivener, B. Bhattacharjee, S. Bishnoi, Changes in microstructure characteristics of cement paste on carbonation, Cem. Concr. Res. 109 (September 2017) (2018) 184–197.
[15] Z. Shi, et al., Experimental studies and thermodynamic modeling of the carbonation

of Portland cement, metakaolin and limestone mortars, Cem. Concr. Res. 88 (2016) 60–72.

[16] M. Serdar, S. Poyet, V.L. Hostis, D. Bjegovi, Carbonation of low-alkalinity mortars: influence on corrosion of steel and on mortar microstructure, Cem. Concr. Res. 101 (May) (2017) 33–45.

[17] F.P. Glasser, T. Matschei, Interactions Between Portland Cement and Carbon Dioxide, ICCC, 2007.

[18] A. Morandeau, M. Thiéry, P. Dangla, Investigation of the carbonation mechanism of CH and C-S-H in terms of kinetics, microstructure changes and moisture properties, Cem. Concr. Res. 56 (2014) 153–170.

[19] M. Castellote, L. Fernandez, C. Andrade, C. Alonso, Chemical changes and phase analysis of OPC pastes carbonated at different CO_2 concentrations, Mater. Struct. Constr. 42 (4) (2009) 515–525.

[20] T.F. Sevelsted, J. Skibsted, Carbonation of C-S-H and C-A-S-H samples studied by ^{13}C, ^{27}Al and ^{29}Si MAS NMR spectroscopy, Cem. Concr. Res. 71 (2015) 56–65.

[21] A. Morandeau, M. Thiéry, P. Dangla, Cement and concrete research impact of accelerated carbonation on OPC cement paste blended with fly ash, Cem. Concr. Res. 67 (2015) 226–236.

[22] S.S. Lucas, V.M. Ferreira, J.L.B. De Aguiar, Incorporation of titanium dioxide nanoparticles in mortars - influence of microstructure in the hardened state properties and photocatalytic activity, Cem. Concr. Res. 43 (1) (2013) 112–120.

[23] R. Sugrañez, et al., Enhanced photocatalytic degradation of NOx gases by regulating the microstructure of mortar cement modified with titanium dioxide, Build. Environ. 69 (x) (2013) 55–63.

[24] J.Z. Bloh, A. Folli, D.E. Macphee, Photocatalytic NO x abatement: why the selectivity matters, RSC Adv. 4 (2014) 45726–45734.

[25] J. Kou, C. Lu, J. Wang, Y. Chen, Z. Xu, R.S. Varma, Selectivity enhancement in heterogeneous photocatalytic transformations, Chem. Rev. 117 (3) (2017) 1445–1514.

[26] L. Yang, A. Hakki, L. Zheng, M. R. Jones, F. Wang, and D. E. Macphee, "Photocatalytic concrete for NOx abatement: supported TiO_2 efficiencies and impacts," Cem. Concr. Res., vol. 116, no. November 2018, pp. 57–64, 2019.

[27] M. Horgnies, I. Dubois-Brugger, E.M. Gartner, NO x de-pollution by hardened concrete and the influence of activated charcoal additions, Cem. Concr. Res. 42 (10) (2012) 1348–1355.

[28] L. Yang, A. Hakki, F. Wang, D.E. Macphee, Photocatalyst efficiencies in concrete technology: the effect of photocatalyst placement, Appl. Catal. B Environ. 222 (August 2017) (2018) 200–208.

[29] X. Zhang, H. Tong, H. Zhang, C. Chen, Nitrogen oxides absorption on calcium hydroxide at low temperature, Ind. Eng. Chem. Res. 47 (11) (2008) 3827–3833.

[30] N.J. Krou, I. Batonneau-Gener, T. Belin, S. Mignard, M. Horgnies, I. Dubois-Brugger, Mechanisms of NOx entrapment into hydrated cement paste containing activated carbon - influences of the temperature and carbonation, Cem. Concr. Res. 53 (x) (2013) 51–58.

[31] C.H. Nelli, G.T. Rochelle, Nitrogen dioxide reaction with alkaline solids, Ind. Eng. Chem. Res. 35 (4) (1996) 999–1005.

[32] Y. Hendrix, A. Lazaro, Q.L. Yu, H.J.H. Brouwers, Influence of synthesis conditions on the properties of photocatalytic titania-silica composites, J. Photochem. Photobiol. A Chem. 371 (October 2018) (2019) 25–32.

[33] X. Gao, S.R. Bare, J.L.G. Fierro, M.A. Banares, I.E. Wachs, Preparation and in-situ spectroscopic characterization of molecularly dispersed titanium oxide on silica, J. Phys. Chem. B 102 (29) (1998) 5653–5666.

[34] Y. Hendrix, A. Lazaro, Q. Yu, J. Brouwers, Titania-silica composites: a review on the photocatalytic activity and synthesis methods, World J. Nano Sci. Eng. 5 (4) (2015) 161–177.

[35] V.S. Smitha, K.A. Manjumol, K.V. Baiju, S. Ghosh, P. Perumal, K.G.K. Warrier, Sol-gel route to synthesize titania-silica nano precursors for photoactive particulates and coatings, J. Sol-Gel Sci. Technol. 54 (2) (2010) 203–211.

[36] X. Zhang, F. Zhang, K.-Y. Chan, Synthesis of titania–silica mixed oxide mesoporous materials, characterization and photocatalytic properties, Appl. Catal. A Gen. 284 (1–2) (2005) 193–198.

[37] M. Montes, F.P. Getton, M.S.W. Vong, P. Sermon, Titania on silica. A comparison of sol-gel routes and traditional methods, J. Sol-Gel Sci. Technol. 8 (1–3) (1997) 131–137.

[38] M. Auroy, et al., Comparison between natural and accelerated carbonation (3% $CO2$): impact on mineralogy, microstructure, water retention and cracking, Cem. Concr. Res. 109 (April) (2018) 64–80.

[39] A.C.A. Muller, K.L. Scrivener, A reassessment of mercury intrusion porosimetry by comparison with1H NMR relaxometry, Cem. Concr. Res. 100 (April) (2017) 350–360.

[40] D.E. Macphee, A. Folli, Photocatalytic concretes — the interface between photocatalysis and cement chemistry, Cem. Concr. Res. 85 (2016) 48–54.

[41] M. Thiery, G. Villain, P. Dangla, G. Platret, Investigation of the carbonation front shape on cementitious materials: effects of the chemical kinetics, Cem. Concr. Res. 37 (7) (2007) 1047–1058.

[42] W.F. Cole, B. Kroone, Carbonate minerals in hydrated portland cement, Nature 7 (4688) (1959) 4688.

[43] P.H.R. Borges, J.O. Costa, N.B. Milestone, C.J. Lynsdale, R.E. Streatfield, Carbonation of CH and C-S-H in composite cement pastes containing high amounts of BFS, Cem. Concr. Res. 40 (2) (2010) 284–292.

[44] Z. Šauman, Carbonization of porous concrete and its main binding components, Cem. Concr. Res. 1 (6) (1971) 645–662 Nov.

[45] E.T. Stepkowska, J.M. Blanes, F. Franco, C. Real, J.L. Pérez-Rodríguez, Phase transformation on heating of an aged cement paste, Thermochim. Acta 420 (1–2 SPEC. ISS) (2004) 79–87.

[46] A. Morandeau, M. Thiéry, P. Dangla, Impact of accelerated carbonation on OPC cement paste blended with fly ash, Cem. Concr. Res. 67 (2015) 226–236.

[47] J.J. Chen, J.J. Thomas, H.M. Jennings, Decalcification shrinkage of cement paste, Cem. Concr. Res. 36 (5) (2006) 801–809.

[48] A. Hakki, L. Yang, F. Wang, D.E. Macphee, The effect of interfacial chemical bonding in TiO2-SiO2 composites on their photocatalytic NOx abatement performance, J. Vis. Exp. (2017) 1–11 no. 125.

[49] B. Weinberger, D.L. Laskin, D.E. Heck, J.D. Laskin, The toxicology of inhaled nitric oxide, Toxicol. Sci. 59 (1) (2001) 5–16.

[50] R. Dillert, A. Engel, J. Große, P. Lindner, D.W. Bahnemann, Light intensity dependence of the kinetics of the photocatalytic oxidation of nitrogen(ii) oxide at the surface of TiO2, Phys. Chem. Chem. Phys. 15 (48) (2013) 20876–20886.

[51] J.J. Thomas, J.J. Chen, A.J. Allen, H.M. Jennings, Effects of decalcification on the microstructure and surface area of cement and tricalcium silicate pastes, Cem. Concr. Res. 34 (12) (2004) 2297–2307.

[52] G. Hüsken, M. Hunger, H.J.H. Brouwers, Experimental study of photocatalytic concrete products for air purification, Build. Environ. 44 (12) (2009) 2463–2474.

[53] S.T. Pham, W. Prince, Effects of carbonation on the microstructure of cement materials: influence of measuring methods and of types of cement, Int. J. Concr. Struct. Mater. 8 (4) (2014) 327–333.